Charm and Beauty production at the LHeC

Presentation at LHeC 3rd workshop

12th November 2010

Chavannes-De-Bogis, Suisse

Olaf Behnke

This is the first draft of a merger of the contributions as submitted for the CDR from

- Gustav Kramer and Hubert Spiesberger
  - D^* mesons in photoproduction
- Gokhan Unel
  - Charm and beauty at a photon proton collider
- Olaf Behnke
  - Charm and beauty in DIS
  - Total cross sections for various processes involving charm, beauty, top and others

Thanks to Gustav, Hubert and Gokhan!

0.0.1 Charm and Beauty production at LHeC

Introduction

The understanding of the dynamics of charm and beauty heavy quark production has been improved considerably over the last years, in particular by the large amount of precise data from the experiments at HERA and the Tevatron. At HERA, heavy quarks are produced in leading order via the Boson Gluon Fusion (BGF) process shown in Figure 1. This process provides direct access to the gluon density in the proton. On the theoretical side, the description of heavy

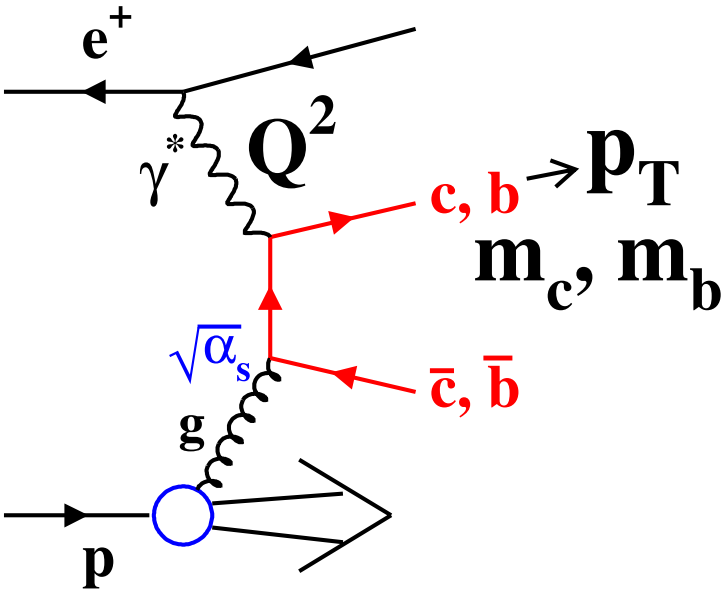

Figure 1: Leading order Boson Gluon Fusion (BGF) diagram for charm and beauty production in *ep*-collisions.

quark production in the framework of perturbative QCD is complicated due to the presence of several large scales like

the heavy quark masses, the transverse momentum p_T of the produced quarks and the momentum transfer Q^2. Depending on the kinematic range considered, the mass m of the heavy quark may have to be taken into account. Different calculational schemes have been developed to obtain predictions from perturbative QCD, depending on the specific kinematical region and the relative importance of the relevant scales. At HERA, it was observed that the charm and beauty production data are described reasonably well over the whole accessible phasespace by Next-to-Leading (NLO) fixed flavour number scheme (FFNS) calculations, where the quark masses are fully accounted for. An LHeC collider with a factor ~ 20 higher squared centre-of-mass energy S would allow to extend the studies to a much larger kinematical phase space. The applicability of the different schemes could be tested up to very high Q^2 and P_T scales, where the NLO FFNS scheme predictions might start to break down. The much higher centre-of-mass energy also allows to probe the gluon density involved in the BGF process at much smaller proton momentum fractions $x_g \leq 10^{-4}$, where it is currently not well known.

The remainder of this article is organised as follows. First the different calculational schemes are introduced. Then phasespace extensions, expected cross sections and implications for QCD tests are discussed for various processes: charm meson photoproduction, charm and beauty produc-

tion at a photon proton collider option of the LHeC, charm and beauty quark production in neutral current DIS and finally total cross sections for various processes involving charm, beauty and also top quarks in the final state. The article concludes with a brief summary.

Calculation schemes for heavy quark productions

In the case of relatively small transverse momentum, $p_T \lesssim m$, the fixed-flavour number scheme (FFNS) is usually applied [1]. Here one assumes that the light quarks and the gluon are the only active flavours within the colliding hadrons (and the photon in the case of photoproduction). In the FFNS the charm quark appears only in the final state. The charm quark mass m can explicitly be taken into account together with the transverse momentum of the produced heavy meson; this approach is therefore expected to be reliable when p_T and m are of the same order of magnitude.

In the complementary kinematical region where $p_T \gg m$, calculations are usually based on the zero-mass variable-flavour-number scheme (ZM-VFNS). This is the conventional parton model approach where the zero-mass parton approximation is applied also to the charm quark, although its mass is not small compared with Λ_{QCD}. In the ZM-VFNS, the charm quark acts also as an incoming parton with its own parton distribution function (PDF) leading to additional direct and resolved contributions. Usually, charm quark PDFs and also the fragmentation functions (FFs), describing the transition of the charm quark to the charmed meson, are defined at an initial scale μ_0 chosen equal to the charm mass m. Then this is the only place, where the charm mass enters in this scheme. The heavy meson is produced not only by frag-

mentation from the charm quark created in the hard scattering process; but also fragmentation from the light quarks and the gluon has to be taken into account. The well-known factorization theorem provides a unique procedure for incorporating the FFs into the perturbative calculations. The predictions obtained in this scheme are expected to be reliable only in the region of large p_T since all terms of the order m^2/p_T^2 are neglected in the hard scattering cross section. For photoproduction, calculations for charm-production in the ZM-VFNS have been performed in Ref. [2].

A unified scheme that combines the virtues of the FFNS and the ZM-VFNS is the so-called general-mass variable-flavour-number scheme (GM-VFNS) [3]. In this approach the large logarithms $\ln(p_T^2/m^2)$, which appear due to the collinear mass singularities in the initial and final state, are factorized into the PDFs and FFs and summed by the well known DGLAP evolution equations. The factorization is performed following the usual $\overline{\rm MS}$ prescription which guarantees the universality of both PDFs and FFs. At the same time, mass-dependent power corrections are retained in the hard-scattering cross sections, as in the FFNS. In order to conform with the $\overline{\rm MS}$ factorization, finite subtraction terms must be supplemented to the results of the FFNS. As in the ZM-VFNS, one has to take into account processes with incoming charm quarks, as well as light quarks and gluons in the final state which fragment into the heavy meson. It

is expected that this scheme is valid not only in the region $p_T^2 \gg m^2$, but also in the kinematic region where p_T is larger than only a few times the charm mass m. The basic features of the GM-VFNS are described in Ref. [4]. Analytic results for the required hard scattering cross sections can be found in Refs. [5].

It is the purpose of this work to present theoretical predictions for the production of D^*-meson production in electron proton scattering at the LHeC. We assume an experimental analysis with data taken in the photoproduction regime, i.e. with an upper limit of $Q^2 \leq 1$ GeV^2. Since the cross section is dominated by low Q^2, our results should not depend too strongly on the precise value of this cutoff and our conclusions still be valid. Details of the calculation can be found in Ref. [4].

The D^*-production cross section $\sigma_{ep}(\sqrt{s})$ at the ep center-of-mass energy $\sqrt{s}$ is related to the photoproduction cross section at center-of-mass energy $W_{\gamma p}$, $\sigma_{\gamma p}(W_{\gamma p})$, through

$$\sigma_{ep}(\sqrt{s}) = \int_{y_{\min}}^{y_{\max}} dy f_{e\gamma}(y) \sigma_{\gamma p}(y\sqrt{s})\,. \tag{1}$$

Here, $f_{e\gamma}$ is the energy spectrum of the exchanged virtual photon which in the Weizsäcker-Williams approximation is given by

$$f_{e\gamma}(y) = \frac{\alpha}{2\pi}\left[\frac{1+(1-y)^2}{y}\ln\frac{(1-y)Q^2_{\max}}{y^2 m_e^2} + 2(1-y)\left(\frac{y m_e^2}{(1-y)Q^2_{\max}} - \frac{1}{y}\right)\right.$$

The photon flux $f_{e\gamma}$ depends on $Q^2_{\max}$ and on $y = E_\gamma/E_e$, the ratio of the energies of the incoming photon and electron, which is determined by the inelasticity $y = Q^2/(2P{\cdot}q)$ where P and q are the 4-momenta of the incoming proton and the

photon. The range of y, $y_{\min} \leq y \leq y_{\max}$ are determined by the cuts in the experimental analysis. For simplicity we have chosen $y_{\min} = 0.1$, $y_{\max} = 0.9$, but these limits can easily be adjusted as soon as more details about the detector layout are known. α is the electromagnetic fine structure constant.

The cross section for direct photoproduction in Eq. (1) is a convolution of the proton PDF, the FF for the transition of a parton to the observed heavy meson, and the cross section for the hard scattering process. For the resolved contribution, an additional convolution with the photon PDFs has to be performed. The hard scattering cross sections are calculated including next-to-leading order corrections. The PDFs and FFs are evolved at NLO. For the photon PDF we use the parametrization of Ref. [6] with the standard set of parameter values and for the proton PDF we have chosen the parametrization CTEQ6.5 [7] of the CTEQ group.

For the FFs we use the set Belle/CLEO-GM of Ref. [8] based on a fit of the combined Belle [9] and CLEO [10] data at $\sqrt{s} = 10.52$ GeV. For similar calculations at HERA we had observed that the photoproduction cross section $d\sigma/dp_T$ are larger by 25−30% in average when using the Belle/CLEO-GM parametrization, as compared to the set Global-GM of Ref. [8]. The strong coupling constant $\alpha_s^{(n_f)}(\mu_R)$ is evaluated with the two-loop formula [11] with $n_f = 4$ active quark flavours and the asymptotic scale parameter $\Lambda^{(4)}_{\overline{\rm MS}} = 328$

MeV, corresponding to $\alpha_s^{(5)}(m_Z) = 0.118$. The charm quark mass is fixed to $m = 1.5$ GeV. We choose the renormalization scale μ_R and the factorization scales μ_F related to initial- and final-state singularities to be $\mu_R = \xi_R m_T$ and $\mu_F = \xi_F m_T$, where $m_T = \sqrt{m^2 + p_T^2}$ is the transverse mass. Variations of the parameters ξ_R and ξ_F can be used to study theoretical scale uncertainties; but in the present work we fix them to the default values $\xi_R = \xi_F = 1$. In Ref. [4], we had studied these scale uncertainties for photoproduction at HERA, as well as uncertainties due to various possible choices for input variables, as for example, the proton and photon PDFs and the D^* FFs and the influence of the charm quark mass.

In our calculation we study various combinations of beam energies. To compare with the situation at HERA, we include, as a reference, the values $E^p = 920$ GeV and $E^e = 27.5$ GeV for proton and electron energies, respectively. For the LHeC we take for the proton energy always $E^p = 7$ TeV and consider the options $E^e = 50$, 100 and 150 GeV. The transverse momentum p_T and the rapidity η of the D^*-meson are varied in the kinematic ranges $5 < p_T < 20$ GeV or $20 < p_T < 100$ and $|\eta| < 2.5$.

Numerical results are shown in Fig. 2 for the differential cross section $d\sigma/dp_T$ integrated over the rapidity $|\eta| \leq 2.5$ and in Fig. 3 for $d\sigma/d\eta$, integrated over the p_T-ranges $5 \leq p_T \leq 20$ GeV and $20 \leq p_T \leq 100$ GeV. The higher center-

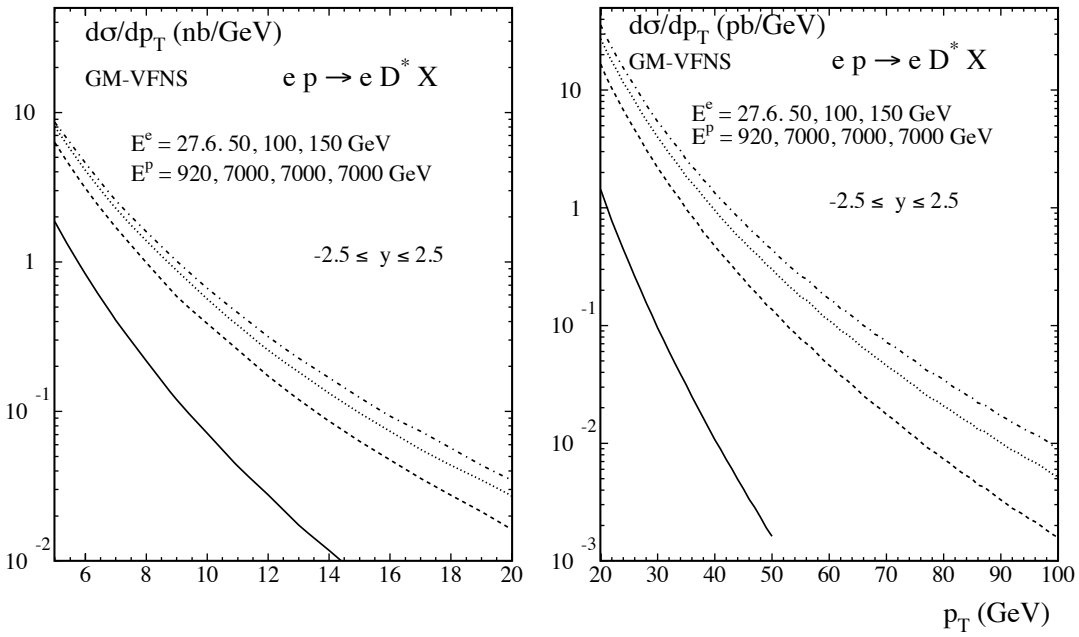

Figure 2: The p_T-differential cross section for the production of D^* mesons at LHeC for different beam energies integrated over rapidities $|\eta| \leq 2.5$. The curves from bottom to top correspond to the combinations of beam energies as indicated in the figure.

of-mass energies available at the LHeC lead to a considerable increase of the cross sections as compared to the situation at HERA. Obviously one can expect an increase in the precision of corresponding measurements and much higher values of p_T, as well as higher values of the rapidity η, will be accessible. Since theoretical predictions also become more reliable at higher p_T, measurements of heavy quark production constitute a promising testing ground for perturbative QCD. One may expect that the experimental information will contribute to an improved determination of the (extrinsic and intrinsic) charm content of the proton and the charm

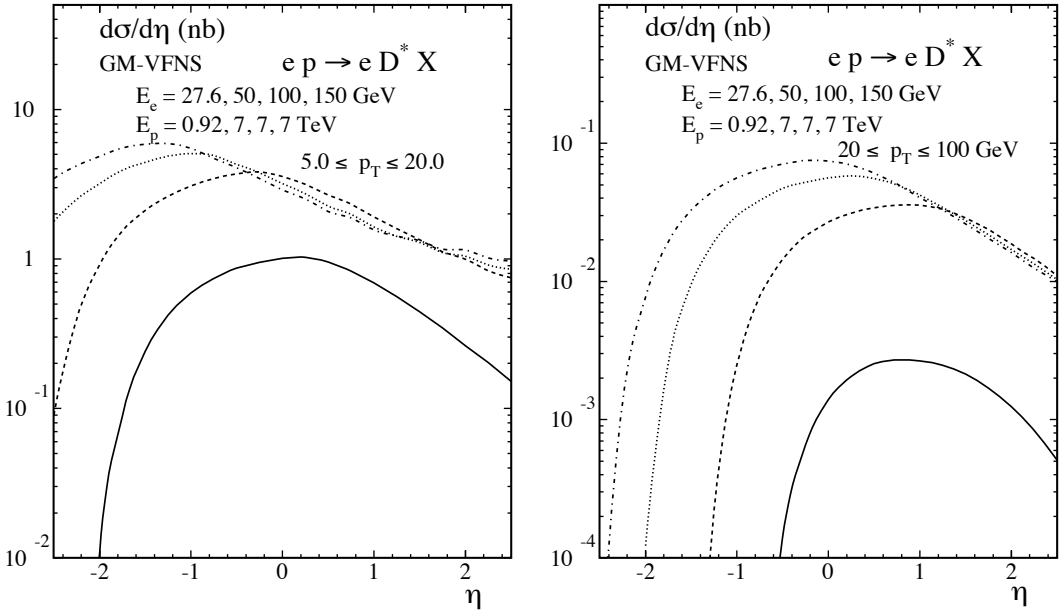

Figure 3: Rapidity distribution of the cross section for the production of D^* mesons at LHeC for different beam energies integrated over the low-p_T range 5 GeV$\leq p_T \leq$ 20 GeV. The curves from bottom to top correspond to the combinations of beam energies as indicated in the figure.

fragmentation functions.

Charm and Beauty production at a photon proton collider

Introduction and Available beams The problem of precise measurement of parton distribution functions (PDF) is yet to be solved for the energy scales relevant for LHC results. One of the needed measurements is the gluon PDF for low momentum fraction: small $x(g)$. The last machine which has probed x(g) was HERA which had a reach of about $x(g) > 10^{-3}$.

The proton beam from LHC can be hit with a high energy electron or photon beam. The photons may be virtual ones from the electron beam resulting in a typical DIS event or they can be real photons originating from the compton back scattering process. In the latter case, the photon spectrum consists of the high energy photons peaking at about 80% of the electron beam energy on the continum of Weizsacker-Williams photons. The type (Linear or Circular) and the energy of the electron machine are yet to be determined. The following study aims to investigate the fesibility of a $x(g)$ measurement with such a machine. The generator level results are obtained using CompHEP and CalcHEP[16] shoftware packages.

Final states interesting for $x(g)$ The final states that can be easily distinguished from the background events and that would give a good measure of the $x(g)$ are $\gamma g \rightarrow q\bar{q}$ where the gluon (g) is from the LHC protons, the photons are from

a new accelerator to be build and the q stands for a heavy quark flavour, such as c quark and possibly b as well. The b quark final states are easier to identify due to b-tagging possibility using a silicon detector. The differential cross sections and the lowest x(g) reach for two electron beam energies (50 and 150 GeV) are shown in Figure 4 in the top row, on the left side for c quarks and on the right side for b quarks. The proton PDF is selected as CTEQ 6L1 and the massses of the c- and $b$quarks are taken as 1.65 GeV and 4.85 GeV, respectively. For comparison the HERA reach is also presented on the same plots. In all cases, higher electron beam energy results in reach to smaller $x(g)$: almost an order of magnitude by going from 50 to 150 GeV. For comparison also cross sections have been simulated for $eg \to eq\bar{q}$ in the DIS kinematic regime at the standard ep collider scenario for LHeC. The observed kinematical reaches are similar to those at a γp collider, however the cross sections are a factor 700 (200) for charm (beauty) lower than those for the γp collider.

Detector effects The angular dependency of the relevant processes is important to estimate the necessary η coverage of the detector and also to estimate the eventual electron machine selection. This dependency is shown in Figure 4 in the bottom row for $c\bar{c}$ (left) and $b\bar{b}$ (right) final states. One can notice that even for an angular loss of only about 5 degrees,

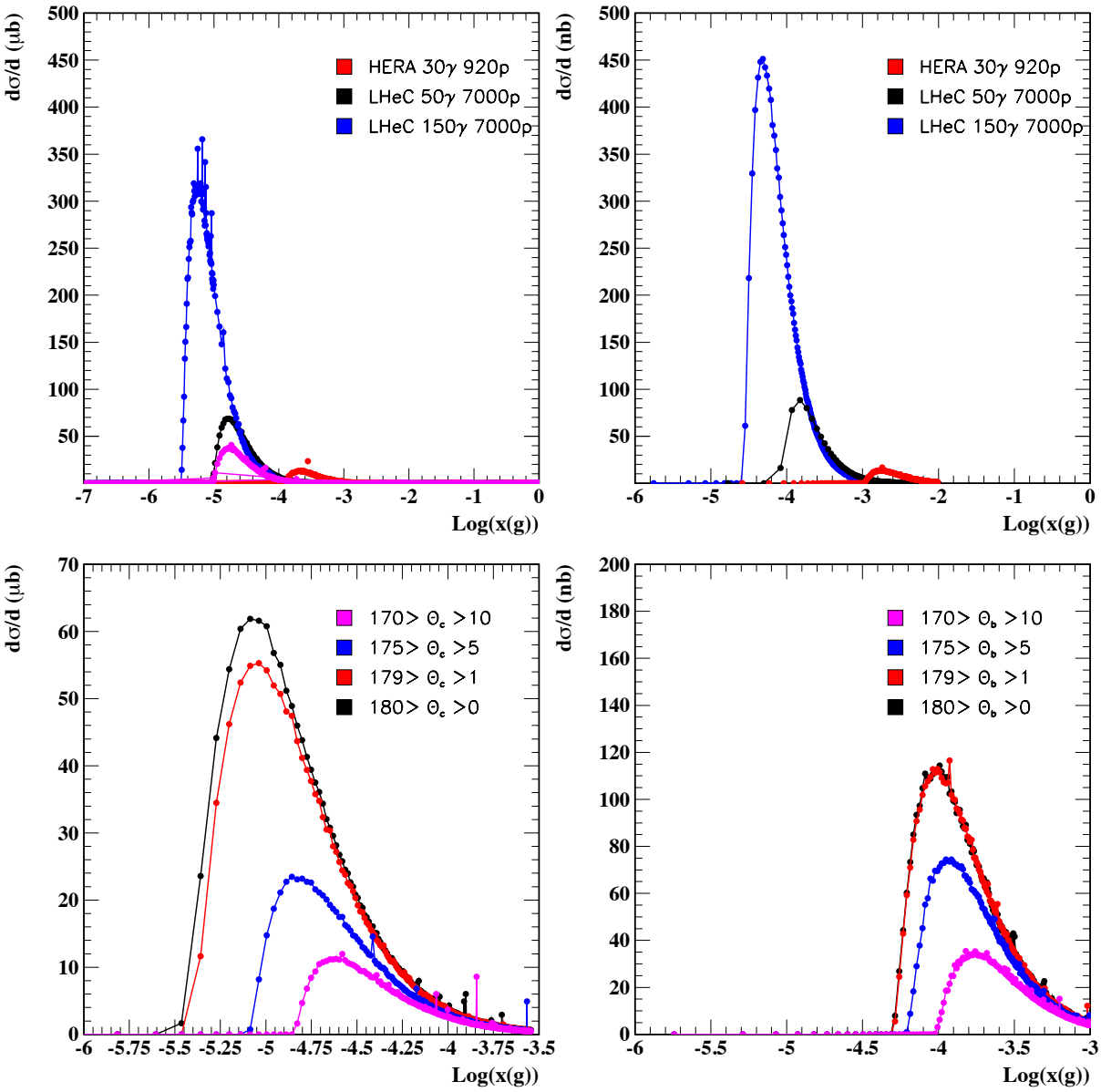

Figure 4: The x(g) reach and differential cross sections at a γp collider for $c\bar{c}$ (left) and $b\bar{b}$ (right) final states, in the top for different photon beam energies and in the bottom for fixed (which????) photon beam energy but various detector polar angle acceptance cuts for the produced heavy quarks.

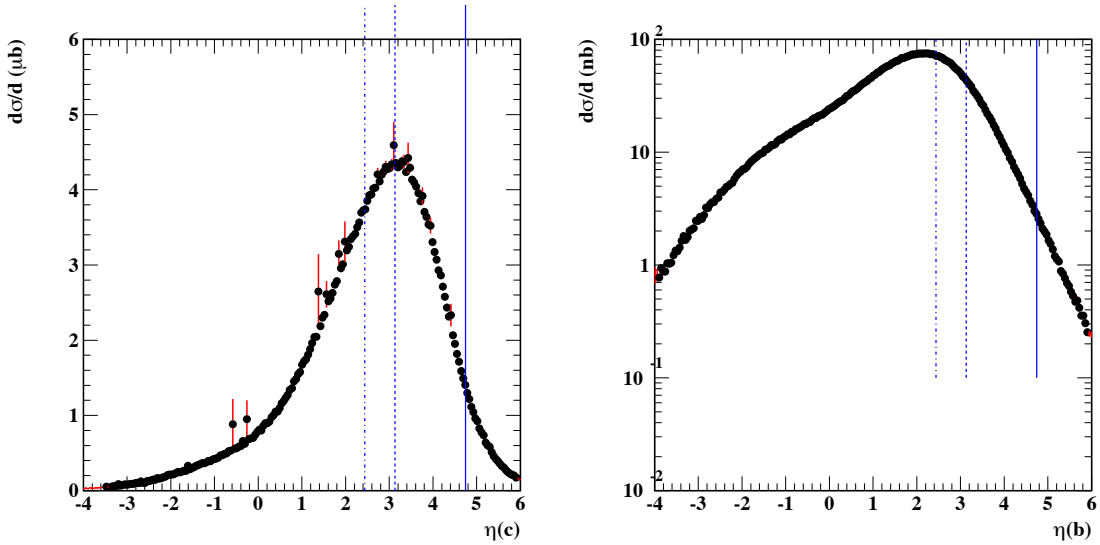

Figure 5: The η dependency of the $c\bar{c}$ (left) and $b\bar{b}$ (right) production cross section in γp collisions.

there is considerable drop in both the cross section and in the $x(g)$ reach. This effect can be understood by considering the η depence of the heavy quark pair production cross section in γp collisions which is shown in Figure 5. The vertical solid line is representative for a 1 degree, the dashed line for a 5 degree and the dot-dashed line is for 10 degree detector. Therefore in order to have the best experimental reach the tracking should have an η coverage up to 5.

Charm and Beauty production in DIS

This section presents predictions for charm and beauty productions in the DIS kinematic regime $Q^2 \geq$ few GeV^2. The results were obtained with the LO+Parton shower Monte Carlo programme RAPGAP3.1 which uses the FFNS massive scheme. The Parton distribution function set CTEQ5L was used. Figure 6 shows the resulting predictions for F_2^{cc} and Figure 7 for F_2^{bb}, in bins of Q^2 and Bjorken x.

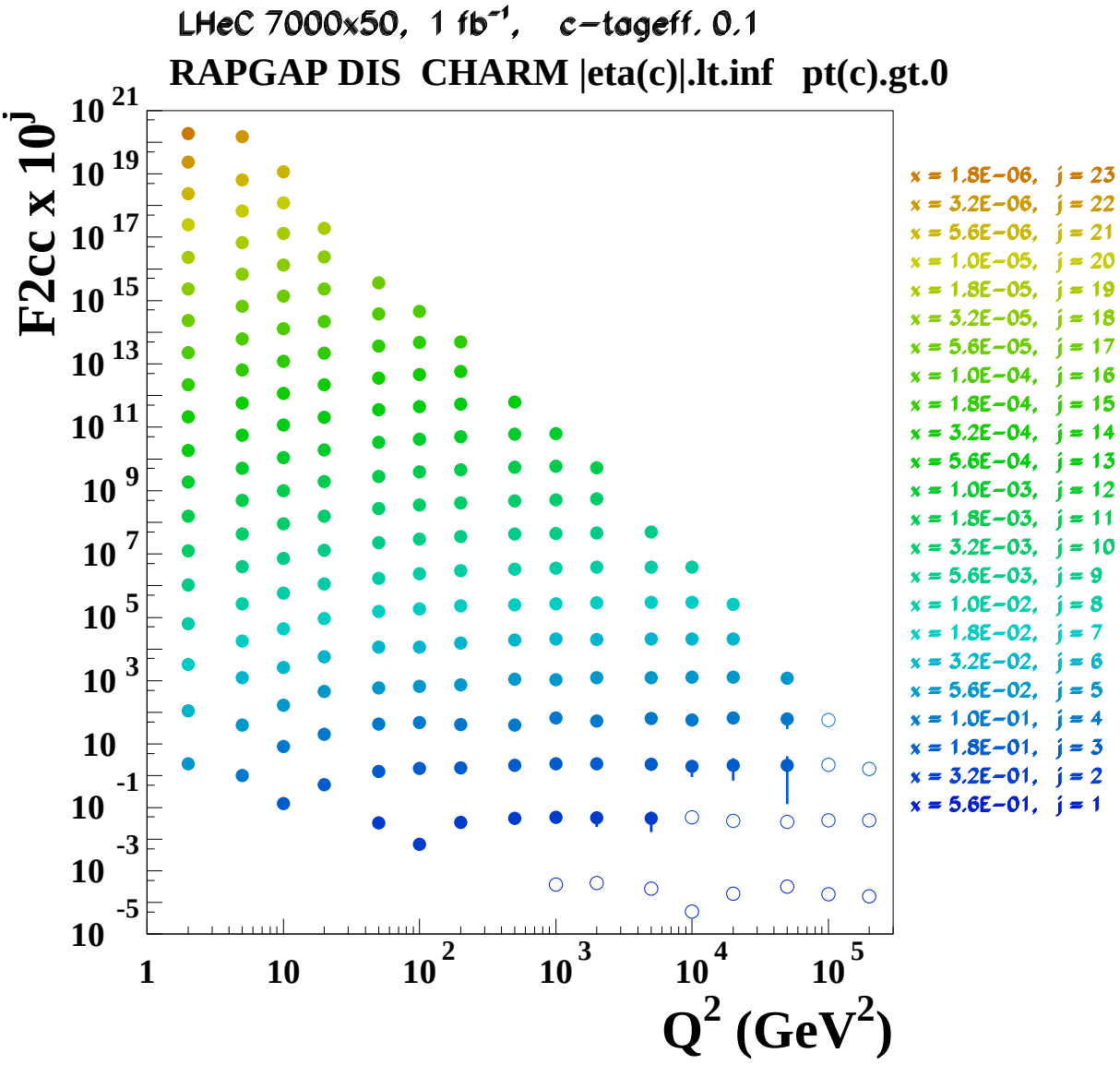

Figure 6: Predictions for the structure functions F_2^{cc}.

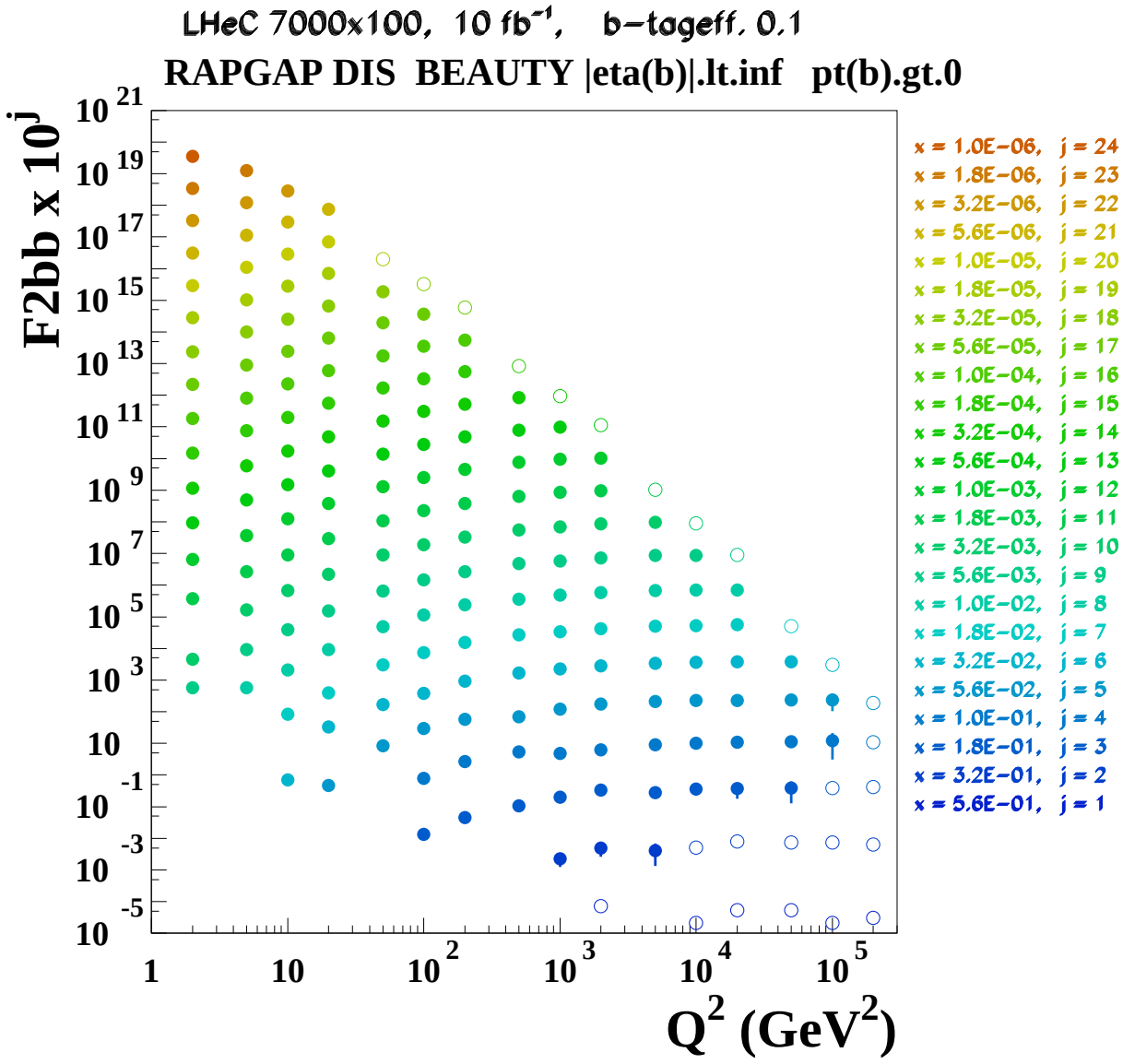

Figure 7: Predictions for the structure functions F_2^{bb}.

Total production cross sections

This section presents total cross sections for various processes at LHeC as a function of the lepton beam energy. Predictions are obtained for: charm and beauty photoproduction and DIS for charged current total cross sections, for the charged current processes $sW \rightarrow c$ and $bW \rightarrow t$ and for top pair production in photoproduction and DIS. Table 1 lists the generated processes, the used Monte Carlo generators, parton distribution functions and other important information. The resulting cross sections are shown in Fig. 8. For comparison also the predicted cross sections for the HERA collider are presented. The cross sections at LHeC are typically about one order of magnitude larger compared to HERA.

Process	Monte Carlo	PDF	Remarks
Charm γp Beauty γp tt γp	PYTHIA6.4	CTEQ6L	Proc. ID 84 m(top) = 170 GeV
Charm DIS Beauty DIS tt DIS	RAPGAP3.1	CTEQ5L	IPRO 12 m(top) = 170 GeV
CC e^+p CC e^-p $sW \rightarrow c$ $sW \rightarrow \bar{c}$ $bW \rightarrow t$ $\bar{b}W \rightarrow \bar{t}$	LEPTO6.5	CTEQ5L	 m(top) = 170 GeV
tt DIS	RAPGAP 3.1	CTEQ5L	

Table 1: Used generator programmes for the predictions of total cross sections at LHeC, shown in Figure 8.

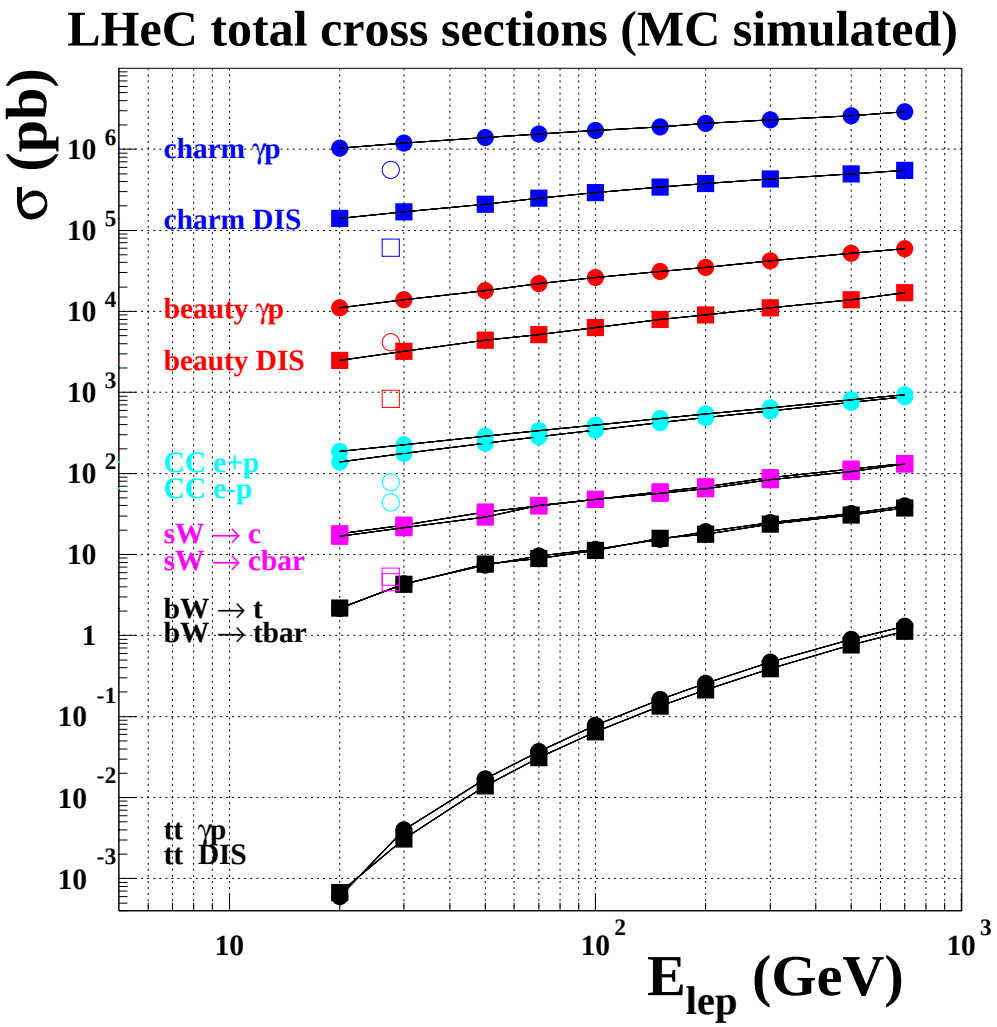

Figure 8: Total production cross sections for various processes at LHeC, involving charm, beauty and top quarks, as a function of the lepton beam energy. All predictions are taken from Monte Carlo simulations, the details are given in Table 1. For comparison also the predicted cross sections at HERA are shown (open symbols).

Summary

The consistent description of heavy quark production from small to large kinematical scales is a challenging problem for perturbative QCD. With the expected increase of the squared centre-of-mass energy S by a factor ~ 20, the LHeC would enable to confront predictions in a much wider phase-space compared to HERA. This has been demonstrated in this article for various processes with charm and beauty quarks in the final state. The presented studies of D^* meson photoproduction show the increased reach to much higher p_T values. The study of charm and beauty quark production at a photon proton collider variant show the extended sensitivity to probe gluons in the proton with momentum fractions as small as $\sim 10^{-5}$, where their density is so far largely unknown. This reach can be only obtained if the LHeC detector is capable of tagging charm and beauty quarks in the very backward region. In DIS (at the standard ep collider option for LHeC) the contributions from events with charm and beauty quarks to F_2, the structure functions F_2^{cc} and F_2^{bb} have been investigated. Much lower x and higher Q^2 values will be accessible compared to HERA. Again, this will allow to probe the gluon density in the proton at smallest momentum fractions and also to test the validity of the different calculation schemes over a large range of Q^2 scales, from $Q^2 \sim m_{c.b}^2$ to $Q^2 \gg m_{c,b}^2$. Finally the total cross sec-

tions for various processes, involving charm, beauty and also top quarks have been studied and found to be typically one order of magnitude (or more) larger than at HERA, making LHeC a genuine multiflavour factory.

Bibliography

[1] B. W. Harris and J. Smith, Phys. Rev. D57 (1998) 2806; S. Frixione, M. Mangano, P. Nason and G. Ridolfi, Phys. Lett. B 348 (1995) 633; S. Frixione, P. Nason and G. Ridolfi, Nucl. Phys. B 545 (1995) 3; and earlier references given there.

[2] J. Binnewies, B. A. Kniehl and G. Kramer, Phys. Rev. D58 (1998) 014014; Z. Phys. C76 (1997) 677; B. A. Kniehl, G. Kramer and M. Spira, Z. Phys. C76 (1997) 689; M. Cacciari and M. Greco, Z. Phys. C69 (1996) 459; Phys. Rev. D55 (1997) 7134.

[3] G. Kramer and H. Spiesberger, Eur. Phys. J. C38 (2004) 309; B. A. Kniehl, G. Kramer, I. Schienbein and H. Spiesberger, Phys. Rev. D71 (2005) 014018.

[4] B. A. Kniehl, G. Kramer, I. Schienbein and H. Spiesberger, Eur. Phys. J. C62 (2009) 365; and references given there.

[5] G. Kramer and H. Spiesberger, Eur. Phys. J. C22 (2001) 289; Eur. Phys. J. C28 (2003) 495; B. A. Kniehl, G.

Kramer, I. Schienbein and H. Spiesberger, Phys. Rev. D 71 (2005) 014018; Eur. Phys. J. C41 (2005) 199.

[6] P. Aurenche, M. Fontannaz, J. Ph. Guillet, Eur. Phys. J. C44 (2005) 395.

[7] CTEQ Collaboration, W. K. Tung, H. L. Lai, A. Belyaev, J. Pumplin, D. Stump and C.-P. Yuan, JHEP0702 (2007) 053.

[8] T. Kneesch, B. A. Kniehl, G. Kramer and I. Schienbein, Nucl. Phys. B799 (2008) 34.

[9] Belle Collaboration, R. Seuster et al., Phys. Rev. D73 (2006) 032002.

[10] CLEO Collaboration, M. Artuso et al., Phys. Rev. D70 (2004) 112001.

[11] C. Amsler et al., Particle Data Group, Phys. Lett. B667 (2008) 1.

[12] ATLAS Detector and Physics Performance Technical Design Report. CERN/LHCC/99-14/15 (1999).

[13] E. Accomando *et al.* [CLIC Physics Working Group], [arXiv:hep-ph/0412251].

[14] R. Ciftci, A. K. Ciftci, E. Recepoglu and S. Sultansoy, Turk. J. Phys. **27**, 179 (2003) [arXiv:hep-ph/0203083].

[15] C. Amsler et al., Phys. Lett. B **667**, 1 (2008).

[16] A. Pukhov, arXiv:hep-ph/0412191 (2004); E. Boos et al. (CompHEP Collaboration), Nucl. Instrum. Meth. A **534**, *250* (2004).